Multichannel Microwave Radiometric Observations at Saipan during the 1990 Tropical Cyclone Motion Experiment

YONG HAN AND DENNIS W. THOMSON

Department of Meteorology, The Pennsylvania State University, University Park, Pennsylvania

(Manuscript received 6 October 1992, in final form 4 May 1993)

ABSTRACT

To estimate mesoscale variations in integrated water vapor, cloud liquid water, and temperature in a tropical region, multiwavelength microwave radiometric observations were carried out over a seven-week period on the island of Saipan during the 1990 Tropical Cyclone Motion Experiment. Methods to combine radiometric and ceilometer measurements were developed to improve both the retrieval accuracies of integrated water vapor and liquid water. The rms difference between the retrieved and radiosonde-measured integrated water vapor was 6% relative to the mean. Compared to radiosondes the temperature profiles retrieved using a linear statistical inversion technique were accurate to 1.28°C. However, since the radiometric temperature profiles were no more accurate than profiles obtained from climatology, the surface-based radiometer provided essentially no new information regarding the environmental temperature profiles.

1. Introduction

During the 1990 Tropical Cyclone Motion Experiment (TCM-90), a ground-based nine-channel microwave radiometer was operated on Saipan, located in a tropical region (15°N, 145°E) in the west-central Pacific Ocean. It was sited there to provide mesoscale, high-temporal-resolution temperature, water vapor, and cloud liquid water measurements. Collocated with the radiometer were a number of other remote sensing and in situ observational instruments. To our knowledge it was the first time that such comprehensive ground-based microwave radiometric observations were made in a tropical region. Thus, one objective of this experiment was to find both the utility and limitations of ground-based microwave radiometric measurements in the tropics. We now know that these observations show some characteristics that differ substantially from similar measurements recorded at midlatitudes. For example, statistical analyses showed that the local climatological variations of tropospheric temperature were comparable to the radiometric retrieval errors typical of midlatitude measurements. Since temperature profile retrieval requires additional temperature information as constraints, usually from an a priori temperature profile ensemble, a practical question arises as to whether or not surface-based radiometers will ever be able to provide temperature profile measurements with accuracies better than those that could be estimated from the climatology.

Corresponding author address: Dr. Yong Han, ERL/ETL/NOAA, R/E/WP5, 325 Broadway, Boulder, CO 80303.

During the past decade studies examining the combined use of ground-based microwave radiometric measurements with those from other remote sensing instruments have showed some encouraging prospects (Westwater et al. 1983; Westwater et al. 1984). The use of combined instruments provides new information to determine the atmospheric variables and, therefore, the accuracy and resolution are improved over those using a radiometer only. Measurements from a radiometer and a ceilometer were combined in this experiment to derive the integrated water vapor and cloud liquid water so that the accuracies were improved. In this paper the experiment description is given in section 2; methods and results in retrieving integrated water vapor and cloud liquid water from combined measurements are presented in section 3. In section 4 the limitations of temperature profile measurements are discussed, followed by conclusions in section 5.

2. Experiment description

The TCM-90 experiment was conducted from 1 August to 21 September 1990. The microwave radiometer was installed adjacent to the Saipan International Airport. Also at the same site was one of the NOAA/ERL/AL (National Oceanic and Atmospheric Administration/Environmental Research Laboratory/Aeronomy Laboratory) 50-MHz wind profilers. Other instruments included a ceilometer and a solar and IR radiometer provided by The Pennsylvania State University (PSU), a 915-MHz wind profiler and a set of baseline surface observation instruments (NOAA/ERL/AL), and an Australian radiosonde receiver de-

veloped by the Bureau of Meteorology Research Centre (BMRC).

The newly developed nine-channel microwave radiometer is one of the components of PSU's large integrated ground-based profiling system (Thomson 1988). It has been assembled to provide continuous remote sensing of atmospheric variables, such as temperature, humidity, wind, and cloud parameters. The radiometer was designed and assembled jointly by faculty and students at PSU and in the department of electrical and computer engineering of the University of Arizona. A block diagram of the radiometer system is shown in Fig. 1 and the system specifications are listed in Table 1. The integrated nine-channel radiometer system consists of four electronically similar and independent radiometer subsystems mounted in the same 17″ × 18″ × 32″ enclosure, an IBM PC-AT personal computer, four microprocessor-based controllers, which serve as interfaces between the various radiometer subsystems and the computer, and a steerable reflector. The system is portable.

The four radiometer subsystems are all of the Dicke-switching type. Two reference loads in each subsystem, one at a temperature of 318 K and the other at 418 K, are used for system gain calibrations. Multichannel operation is realized by using several Gunn oscillators. Radiometer 1 and radiometer 2, each having three channels, operate at six frequencies located in the 60-GHz oxygen absorption band. Radiometer 2 operates at 31.65 GHz in a "window" region, and radiometer 3 operates at 22.235 and 24.1 GHz in the 22.235-GHz water vapor absorption band. The four microcontrollers, each consisting of two 12-bit A/D (analog to digital) convertors, a digital signal processor (DSP), and a single board computer (SBC) are responsible for the frequency selection and the sampling of the three radiation sources (antenna and two reference loads) as well as various physical temperature measurements in the radiometer subsystems. All samples are averaged by the microcontrollers before being sent to the host computer. The host computer controls and communicates with the microcontrollers. The data received by the computer are further processed, and then stored and displayed in real time on the monitor screen in both graphic and tabular forms. The host computer also controls the steerable reflector. The reflector, a solid aluminum plate, is canted at 45° on an axle driven by a microstepping motor. It directs the sky radiation to the radiometer. The radiometer is usually positioned in an air-conditioned environment, horizontally pointing through a low-loss Teflon window to the reflector. The steerable reflector simplifies performing measurements of the radiometric brightness temperature as a function of zenith angle, that is, performing "tipping curves," so that the atmospheric information from slant paths can be obtained. This scanning capability thus provides a means by which those channels with low atmospheric attenuations can be calibrated.

During the TCM-90 experiment, the system operating mode was set such that each recorded radiation datum was an average of 2048 samples and, thus, a temporal resolution of 13 s. These data were later further averaged over 5 min. The six high-frequency channels (oxygen channels) were field calibrated using radiosonde profiles, a radiative transfer model (Liebe 1985), and a blackbody absorber. The three low-frequency channels (vapor–liquid channels) were calibrated using the tipping curve measurements at several elevation angles (Hogg et al. 1983). Both calibrations were accomplished under relatively clear sky conditions. To ensure that the two kinds of calibrations were consistent, the calibrated brightness temperatures from the vapor–liquid channels on the clear sky conditions were compared with those calculated from the radiative

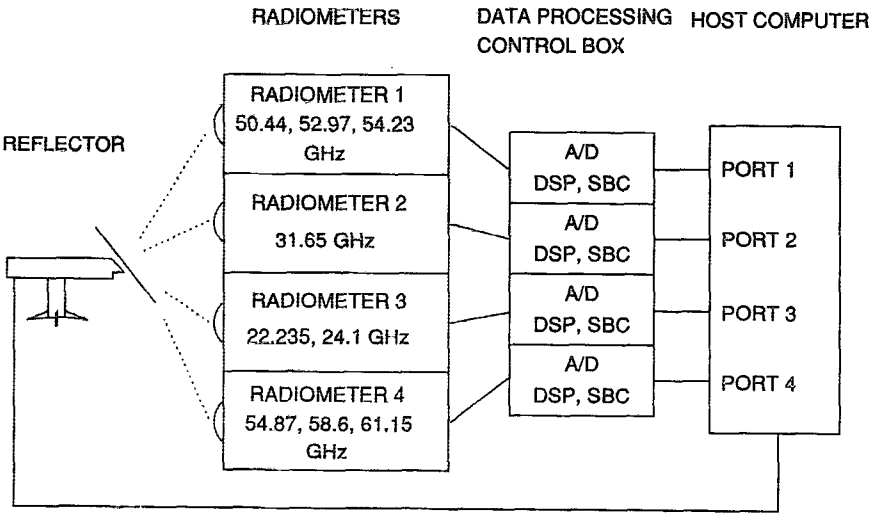

FIG. 1. Radiometer system block diagram.

TABLE 1. Radiometer system specifications.

	Radiometer 1	Radiometer 2	Radiometer 3	Radiometer 4
Frequency (GHz)	50.4, 53.0, 54.2	31.7	22.2, 24.1	54.9, 58.6, 61.2
Antenna beamwidth (deg)	5.0	5.0	5.0	5.0
First sidelobe level (dB)	25	20	22	26
Intermediate frequency bandpass (MHz)	10–205	10–215	10–215	10–215
System noise temperature (K)	1557.9	541.2	463.4	1643.4
System sensitivity (K)	0.319	0.092	0.108	0.329

transfer model and radiosonde profiles. There was no serious systematic bias.

The ceilometer (Albrecht et al. 1990) used to measure the cloud-base height is an active sensor that uses a low-powered gallium arsenide laser diode operating at a wavelength of 0.904 μm. The pulse repetition rate varies between 620 and 1120 Hz in order to maintain a constant averaged power. The cloud-base height with temporal and spatial resolutions of 30 s and 15 m, respectively, is obtained from an averaged return power profile. To match the 5-min-averaged radiometric data, the measurements of cloud base heights were also averaged over 5 min.

Radiosondes were routinely launched twice a day but increased to four times a day during several intensive observational periods (IOPs). The BMRC group launched a total of 125 radiosondes at Saipan during the TCM-90 experiment. Among them, 113 balloons reached a height above 400 mb and 105 ascended to over 100-mb pressure altitude. A balloon took about 27 min to arrive at the 400-mb level and about 30 min more to reach 100 mb.

A serious impediment to reliable system operation during the experiment was the local AC power supply for the site. Not only was it unstable, it often suddenly switched off and on without warning. This off–on operation seriously compromised the radiometer's operation and the problem was not solved until August 15 when a battery backup was installed. Another problem was contamination of the 54.9-GHz channel by radiofrequency from some unknown external source. None of the data recorded on this channel was used for inversion purposes. Continuous operation of the radiometer and ceilometer were interrupted only by the above mentioned ac power problem and for a few minutes each day for archiving and data analysis.

June to October is the rainy season on Saipan. During the entire TCM experiment, the sky consistently, day and night, had scattered convective clouds, moving with the prevailing wind. Intermittently, tropical storms with organized rainbands brought heavy rain. Because of the oceanic regulation and high moisture content, the variations of the low-level air temperature were very small compared to those typically observed at midlatitudes. Figure 2 shows the mean and standard deviation of the temperature profiles from the radiosondes launched at Saipan during this experiment. The overall standard deviation (i.e., the average of the standard deviation at each level) below 400 mb was only 0.9°C. The mean and standard deviation of humidity

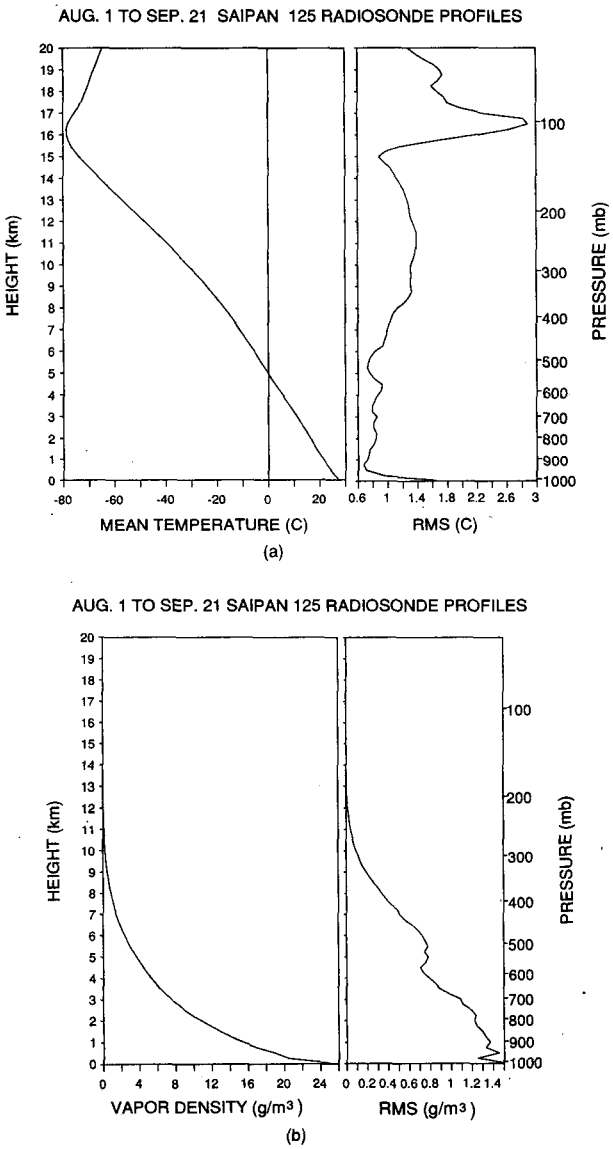

FIG. 2. Means and standard deviations of (a) temperature profiles and (b) water vapor density.

profiles are also shown in Fig. 2. The integrated water vapor derived from these profiles had an average of 5.7 cm with a standard deviation of 0.56 cm.

3. Determination of integrated water vapor and cloud liquid water from combined radiometric and ceilometer measurements

The integrated water vapor V and cloud liquid water L can be derived from radiometric measurements at two frequencies, one relatively sensitive to water vapor and the other relatively sensitive to clouds. Several inversion techniques have been developed to derive V and L from the radiance measurements. Experiments have shown that the rms accuracy in determination of V is comparable to or better than that of radiosondes (Hogg et al. 1983). However, the accuracy of L is very difficult to evaluate due to the lack of "ground truth." Snider et al. (1980) provided an alternative method that compared cloud liquid water, derived from the absorption of a microwave satellite signal, with that measured by a ground-based microwave radiometer. The rms difference was 0.28 mm.

Almost all the inversion techniques treat V and L as functions of the observed brightness temperatures only. However, there are other atmospheric variables, such as temperature and pressure, that also potentially contribute to the brightness temperatures. Generally, these variables are either neglected or treated as parameters assigned constant values. Variations of these variables often do contribute errors in the retrievals (Westwater 1978). Although statistical methods have been developed to reduce the errors by constraining the solutions, variations in these variables still contribute error in the retrievals. Improvement of the retrieval accuracy may be made if uncertainties in determination of these variables are reduced. In this experiment, a method was developed and applied to retrieve V and L from combined radiometric and ceilometer measurements. By this method, two parameters, the cloud absorption coefficients and mean radiating temperatures used in the inversion equations, can be determined from the measurements and, therefore, the retrieval accuracy is improved. In the following, we first describe the method, then discuss its impact on the retrieval accuracy, and finally present experimental results. Since it has been common practice to derive V and L from dual-channel measurements, we applied this method to the radiometric database from the two channels, 22.2 and 31.7 GHz. We chose the 22.2-GHz rather than 24.1-GHz channel as the 22.2-GHz channel was less noisy than the 24.1-GHz channel during this experiment.

a. Method

Here, V and L may be derived using a simple physical inversion technique (Westwater 1978) as

$$V = \frac{\bar{k}_{L,\nu_2}\tau'_{\nu_1} - \bar{k}_{L,\nu_1}\tau'_{\nu_2}}{\bar{k}_{V,\nu_1}\bar{k}_{L,\nu_2} - \bar{k}_{V,\nu_2}\bar{k}_{L,\nu_1}}, \quad (1)$$

$$L = \frac{-\bar{k}_{V,\nu_2}\tau'_{\nu_1} + \bar{k}_{V,\nu_1}\tau'_{\nu_2}}{\bar{k}_{V,\nu_1}\bar{k}_{L,\nu_2} - \bar{k}_{V,\nu_2}\bar{k}_{L,\nu_1}}. \quad (2)$$

In the equations, 1 and 2 refer to the water vapor–sensitive and cloud-sensitive channels, respectively, and $\bar{k}_{V,\nu}$ and $\bar{k}_{L,\nu}$ are path-averaged water vapor and liquid water absorption coefficients, defined as

$$\bar{k}_{V,\nu} = \frac{1}{V}\int_0^{\infty} \rho_V k_{V,\nu} dz, \quad (3)$$

$$\bar{k}_{L,\nu} = \frac{1}{L}\int_0^{\infty} w_L k_{L,\nu} dz, \quad (4)$$

where $k_{V,\nu}$ and $k_{L,\nu}$ are the mass absorption coefficients of water vapor and liquid, and ρ_V and w_L are the water vapor density and liquid water content. Here, τ'_ν are the optical depths of water vapor and cloud liquid and may be derived from the mean radiating temperature $T_{mr,\nu}$ and the observed brightness temperature $T_{b,\nu}$ as

$$\tau'_\nu = \ln\left(\frac{T_{mr,\nu} - T_{\rm bb}}{T_{mr,\nu} - T_{b,\nu}}\right) - \tau_{d,\nu'} \quad (5)$$

where $\tau_{d,\nu}$ is the dry-air optical depth and $T_{\rm bb}$ is the "big bang" cosmic background of 2.75 K. The mean radiating temperature $T_{mr,\nu}$ is defined as

$$T_{mr,\nu} = \frac{\int_0^{\tau_{\nu,\infty}} Te^{-\tau_\nu} d\tau_\nu}{1 - e^{-\tau_{\nu,\infty}}}, \quad (6)$$

where τ_ν is an optical path.

A modest improvement over the physical inversion technique can be achieved by applying a statistical constraint to the solution. One such technique is the linear statistical inversion. It may be written as (Rodgers 1976)

$$(V, L)^{\rm T} = (V_0, L_0)^{\rm T} + \mathbf{S}_0\mathbf{K}^{\rm T}(\mathbf{K}\mathbf{S}_0\mathbf{K}^{\rm T} + \mathbf{S}_\epsilon)^{-1}[\tau' - \mathbf{K}(V_0, L_0)^{\rm T}], \quad (7)$$

where V_0 and L_0 are climatological means of V and L, $\mathbf{S}_0$ is the corresponding covariance, $\mathbf{S}_\epsilon$ is the error matrix of the effective measurement vector $\tau' = (\tau'_{\nu 1}, \tau'_{\nu 2})$, and

$$\mathbf{K} = \begin{pmatrix} \bar{k}_{V,\nu_1} & \bar{k}_{L,\nu_1} \\ \bar{k}_{V,\nu_2} & \bar{k}_{L,\nu 2} \end{pmatrix}. \quad (8)$$

The statistical inversion technique was applied to derive V and L in this experiment. However, because of the simplicity and its physical transparency, the physical inversion algorithm was used to predict the retrieval accuracy.

The use of (1), (2), and (7) to derive V and L from measurements of $T_{b,\nu}$ requires knowledge of absorption

coefficients, dry-air attenuations, and mean radiating temperatures. Usually, these parameters are predetermined and assumed constant. However, they vary with the changes in the atmospheric state. Westwater (1978) has provided some estimation on how the variations of these parameters affect the inversion accuracy. A brief discussion on the relationships of the cloud absorption coefficient $\bar{k}_{L,\nu}$ and the mean radiating temperature $T_{mr,\nu}$ with the cloud parameters is given below.

At a specified microwave frequency, for most nonprecipitating clouds, the Rayleigh approximation applies and the mass absorption coefficient is a function of cloud temperature only. However, because of the vertical variations of the cloud temperature, the path-averaged mass absorption coefficient, defined in (4), is also dependent on the cloud thickness, vertical distribution of cloud temperature, and liquid water content. These cloud parameters are highly variable in time and, hence, cause variations in $\bar{k}_{L,\nu}$. For example, a 10°C change in cloud temperature, which is not uncommonly observed at middle latitudes, could cause a change of about 27% in $\bar{k}_{L,\nu}$. Assuming a cloud temperature lapse rate of 5°C km^{-1} and a constant liquid content profile, $\bar{k}_{L,\nu}$ changes about 13%, if the cloud thickness is changed from 0.2 to 2 km. Assuming a cloud with thickness of 2 km and a 5°C temperature lapse rate, a change of 4% in $\bar{k}_{L,\nu}$ arises if the vertical distribution of the cloud liquid content is shifted from a constant profile to a moist adiabatic profile.

The mean radiating temperature $T_{mr,\nu}$, defined in (6), is determined by the atmospheric temperature profile and atmospheric, including cloud, absorptions. The influence of clouds on $T_{mr,\nu}$ depends also on cloud height and thickness. Since $T_{mr,\nu}$ is an average of temperature profile $T(z)$, weighted by the function $(de^{-\tau_\nu})$, a function with high-altitude clouds will weigh the colder portion of the temperature profile more heavily than one without clouds and, hence, may result in a lower value of $T_{mr,\nu}$. A function with lower-altitude clouds may result in $T_{mr,\nu}$ larger than when there are no clouds.

To account for the cloud-caused variations in $\bar{k}_{L,\nu}$ and $T_{mr,\nu'}$ we should regard them as variables to be determined through measurements. With certain assumptions, joint measurements by a radiometer and a ceilometer can provide the information necessary to calculate $\bar{k}_{L,\nu}$ and $T_{mr,\nu}$.

1) Calculation of $\bar{k}_{L,\nu}$

The cloud-base height measured by the ceilometer is one of the parameters that determines $\bar{k}_{L,\nu}$. Another parameter, the cloud-base temperature, can be obtained if the cloud-base height measurements are incorporated with a simultaneously measured temperature profile. The temperature profiles can be provided by a microwave radiometer with oxygen-sensitive channels, such as the one we used, or by other remote sensing instruments, such as a radio acoustic sounding system or an IR thermometer. For this experiment we used a climatological mean profile as the variations of the tropical air temperature, discussed later in section 4, are very small. The remaining parameters were obtained based on these assumptions: (a) the cloud liquid water content was moist adiabatic and a linear function of height above cloud base, (b) the temperature lapse rate in cloud was moist adiabatic, and (c) there was no water to ice phase change in the cloud. These lead to the cloud liquid water content and thickness given as (Albrecht et al. 1990)

$$w_L(z) \simeq \bar{\rho}\,\Gamma_L(z - z_b), \tag{9}$$

$$\Delta z_c = z_t - z_b = \left(\frac{2L^0}{\Gamma_L \bar{\rho}}\right)^{1/2}. \tag{10}$$

In (9) and (10), Γ_L is defined as the derivative of the adiabatic liquid water mixing ratio to the altitude variable z and $\bar{\rho}$ is the air density. Both are the averages in the cloud layer. Here, z_b and z_t are heights of cloud base and top. The pressure profile needed for estimating Γ_L and $\bar{\rho}$ is given by the climatological mean. The integrated liquid water L^0 in (10) is obtained by an initial retrieval from the radiometric measurements using (7), in which $\bar{k}_{L,\nu}$ and $T_{mr,\nu}$, as well as other parameters, are climatological means. Knowing cloud temperature, w_L and Δz_c, we can calculate the cloud absorption $\bar{k}_{L,\nu}$ from (4).

In reality, a moist-adiabatic water content is rarely reached in clouds. However, the case studies by Albrecht et al. (1990) and Politovich et al. (1992) suggested that it was a reasonable approximation. In addition, since this approximation affects $\bar{k}_{L,\nu}$ through the cloud thickness Δz_c and the ratio of the water content w_L to the total water L, a small or moderate departure from the moist-adiabatic water content will not be a serious problem. Assuming the error in estimating the cloud-base temperature is 2°C and the error in the initial retrieval of L is 30%, errors in $\bar{k}_{L,\nu}$ at 22.2 and 31.7 GHz as a function of L are shown in Fig. 3. As a comparison, the climatological variation of $\bar{k}_{L,\nu}$ in the summer in the experimental region is 0.132 at 22.2 GHz and 0.251 at 31.7 GHz, about five times the values shown in Fig. 3.

2) Calculation of $T_{mr,\nu}$

Here, $T_{mr,\nu}$ can be expressed in a form suitable for accounting for the cloud variations. After dividing the integral in (6) into three parts, corresponding to the layer below the cloud, the cloud layer and the layer above the cloud, and knowing that the optical path τ_ν is the sum of the optical paths of dry air, water vapor, and cloud, we can write (6) in the form

$$T_{mr,\nu} = T^0_{mr,\nu} + dT_{mr,\nu}, \tag{11}$$

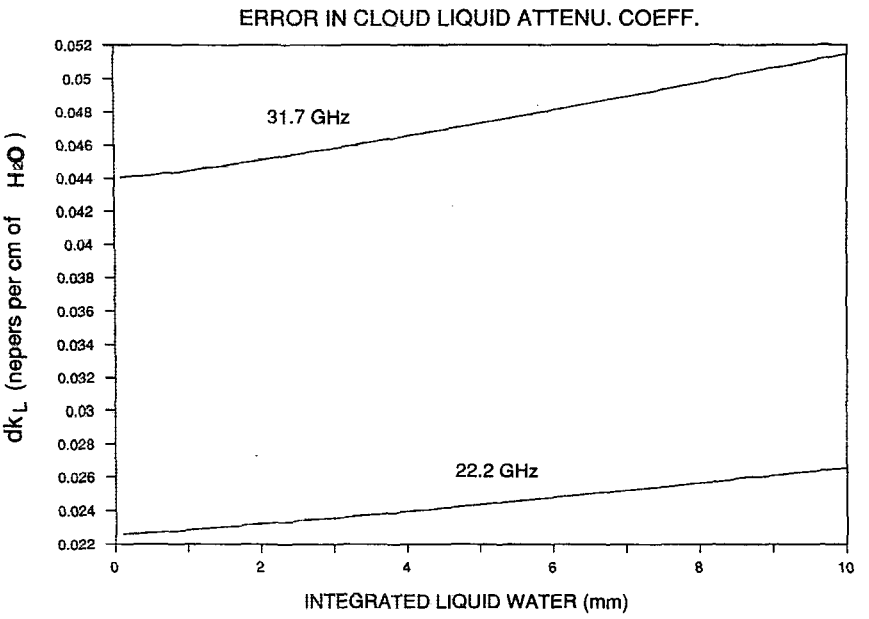

FIG. 3. Errors in estimation of path-averaged cloud absorption coefficients as a function of integrated liquid water for a specified cloud height 700 m.

where

$$dT_{mr,\nu} = \frac{[1 - e^{-\tau_{L,\nu}(z_b,z_t)}]}{[1 - e^{-\tau_\nu(0,\infty)}]}\,[e^{-\tau_\nu^0(0,z_t)}T_{\text{cld}} + (1 - e^{\tau_\nu^0(0,z_t)})T_{mr,\nu}^0(0, z_t) - T_{mr,\nu}^0(0, \infty)]. \quad (12)$$

In above equations, $T_{mr,\nu}^0(0, z)$ and $\tau_\nu^0(0, z)$ are the mean radiating temperature and optical path between the surface and the level z under cloud-free condition, T_{cld} is the vertical-averaged cloud temperature. The first term on the right side of (11) is the mean radiating temperature under cloud-free conditions and the second term is a contribution due to the presence of the cloud.

Here, $T_{mr,\nu}^0(0, z)$ and $\tau_\nu^0(0, z)$ depend on the state of the atmospheric layer between the surface and the level z. They were approximated by the climatological means; $\tau_{L,\nu}(z_b, z_t)$ was determined in a way similar to that for $\bar{k}_{L,\nu}$; and T_{cld} was assumed the value of the arithmetic mean of the cloud base and top temperatures. An example of $dT_{mr,\nu}$ as a function of L is shown in Fig. 4 for a specified cloud base and height of 700 m. In general, the magnitude and sign of $dT_{mr,\nu}$ depend on the cloud base height, temperature, and thickness.

b. Error analysis

Following the method suggested by Westwater (1978), we evaluated the accuracies of the physical inversions with and without corrections to $\bar{k}_{L,\nu}$. Let p_i and Δp_i represent the various parameters and the departures from the means. The errors in physical retrievals of V and L may be estimated as

$$E[(\Delta V)^2] = \sum \frac{\partial V}{\partial p_i}\frac{\partial V}{\partial p_j} E(\Delta p_i \Delta p_j), \quad (13)$$

$$E[(\Delta L)^2] = \sum \frac{\partial L}{\partial p_i}\frac{\partial L}{\partial p_j} E(\Delta p_i \Delta p_j), \quad (14)$$

where $E[\ ]$ represents the expectation. Measurement errors of the brightness temperatures were assumed to be 1 K and independent of one another and of the errors in the other parameters. The means, standard deviations, and correlation coefficients of these parameters, as listed in Table 2, were obtained from an a priori ensemble of radiosonde profiles and the radiative transfer model. The radiosondes were launched from Guam, which is located about 100 miles south of Saipan, in August and September during 1984–88. In the radiative transfer model, cloud layers were stipulated when the relative humidity exceeded 95% and the cloud liquid water content was assumed moist adiabatic. When calculating the retrieval errors with the corrections of $\bar{k}_{L,\nu}$, we assumed that the error in cloud-base temperature was 2°C and error in the initial retrievals L^0 was 30%; errors in $\bar{k}_{L,\nu_1}$ and $\bar{k}_{L,\nu_2}$ were correlated with each other but uncorrelated with those in other parameters.

Figure 5 shows errors in retrieved V and L with and without corrections to $\bar{k}_{L,\nu}$ as a function of L for a specified V of 5.6 cm and a cloud-base height of 700 m. The accuracy of the retrieved L is improved by more than 50% in general. We also calculated retrieval errors given different vertical distributions of cloud liquid water content. The situation was not significantly dif-

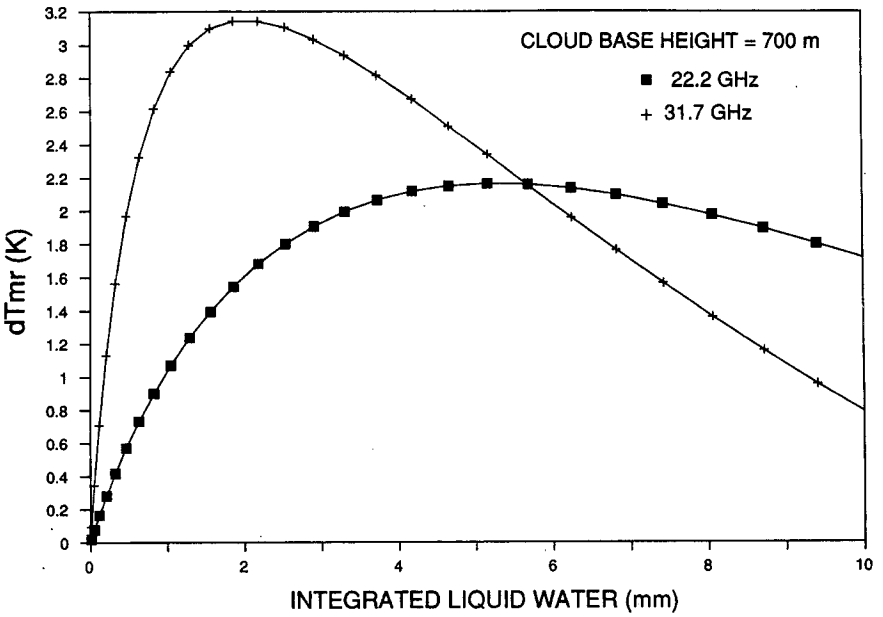

FIG. 4. Differences between cloudy and cloud-free mean radiating temperatures as a function of integrated liquid water for a specified cloud height 700 m.

ferent from that shown in Fig. 5 when L was less than 1 cm. The improvement in retrieval accuracy of V was slight and not as good as that suggested by Westwater (1978) for the case at middle latitudes. The insignificant improvement was due to the following facts: (a) V is affected by the ratio of $\bar{k}_{L,\nu_1}$ to $\bar{k}_{L,\nu_2}$, not to their individual values; (b) $\bar{k}_{L,\nu_1}$ and $\bar{k}_{L,\nu_2}$ are highly correlated; and (c) variations in $\bar{k}_{L,\nu}$ are relatively small compared to those at middle latitudes.

The influence of $T_{mr,\nu}$ on the retrieval accuracy takes place through the effective measurement τ'_ν. At $V = 5.6$ cm and $L = 0.2$ cm, 2°C correction to $T_{mr,\nu}$ will reduce the uncertainty in τ'_ν by about 0.0047 Np at $\nu = 22.2$ GHz and 0.00328 Np at $\nu = 31.7$ GHz. These are equivalent to a reduction of uncertainty in brightness temperature measurements by about 0.7 K. Using (12) and (13) we estimated that in the range of $L = 0.1$–0.5 cm, a correction of $T_{mr,\nu}$ by 1–3 K will reduce the retrieval error by about 0.5%–2% for both V and L.

c. *Experimental results*

During this experiment, errors in the radiometric data were primarily due to local ac power outages and rain. Erroneous data were eliminated when the brightness temperature at 31.7 GHz exceeded 160 K or the inspected data at a given frequency differed significantly from the values predicted by two other selected channels. The predicted values were obtained from linear regressions (Westwater et al. 1990) constructed from the data under nonprecipitating conditions. Two additional channels, 24.1 and 50.4 GHz were used for this purpose.

The inversion of each dataset consisted of the following steps:

(a) obtain the initial retrievals of V and L using (7), in which $\bar{k}_{L,\nu}$ and $T_{mr,\nu}$ are given by climatological means, and the effective measurement errors are estimated as

$$\epsilon_\nu^2 = \left(\frac{\partial \tau_\nu}{\partial T_{b,\nu}} \Delta T_{b,\nu}\right)^2; \qquad (15)$$

TABLE 2a. Climatological means and standard deviations used for error analysis. Units: T_{mr}—kelvins, τ—nepers, $\bar{K}_V$, or $\bar{K}_L$—nepers per centimeter of H_2O.

$T_{mr,22}$	2.872×10^{2}
$\tau_{d,22}$	1.211×10^{-2}
$\bar{K}_{V,22}$	6.680×10^{-2}
$\bar{K}_{L,22}$	6.406×10^{-1}
$T_{mr,32}$	2.878×10^{2}
$\tau_{d,32}$	2.277×10^{-2}
$\bar{K}_{V,32}$	1.917×10^{-2}
$\bar{K}_{L,32}$	1.268×10^{0}
$dT_{mr,22}$	2.332×10^{0}
$d\tau_{d,22}$	8.325×10^{-5}
$d\bar{K}_{V,22}$	4.213×10^{-3}
$d\bar{K}_{L,22}$	1.322×10^{-1}
$dT_{mr,32}$	2.037×10^{0}
$d\tau_{d,32}$	1.554×10^{-4}
$d\bar{K}_{V,32}$	5.327×10^{-4}
$d\bar{K}_{L,32}$	2.510×10^{-1}

TABLE 2b. Correlation coefficients used for error analysis.

	$T_{mr,22}$	$\tau_{d,22}$	$\bar{K}_{V,22}$	$\bar{K}_{L,22}$	$T_{mr,32}$	$\tau_{d,32}$	$\bar{K}_{V,32}$	$\bar{K}_{L,32}$
$T_{mr,22}$	1.000							
$\tau_{d,22}$	−0.094	1.000						
$\bar{K}_{V,22}$	0.217	−0.1651	1.000					
$\bar{K}_{L,22}$	−0.364	0.041	0.179	1.000				
$T_{mr,32}$	0.550	−0.256	−0.1839	−0.780	1.000			
$\tau_{d,32}$	0.054	0.976	−0.123	0.053	−0.168	1.000		
$\bar{K}_{V,32}$	0.054	0.164	−0.608	−0.316	0.386	0.158	1.000	
$\bar{K}_{L,32}$	−0.363	0.041	0.179	1.000	−0.779	0.054	−0.314	1.000

(b) if L exceeds a certain value (0.01 mm), go to the next step, otherwise output V and L;

(c) if the ceilometer indicates "cloud," go to the next step, otherwise output V and L;

(d) calculate $\bar{k}_{L,\nu_1}$, $\bar{k}_{L,\nu_2}$, $T_{mr,\nu 1}$, and $T_{mr,\nu 2}$;

(e) calculate V and L in the same way as step (a) but with the new values of $\bar{k}_{L,\nu}$ and $T_{mr,\nu}$.

A time series of retrieved V, compared with radiosonde-derived V, and retrieved L is shown in Fig. 6. A scatterplot of retrieved versus radiosonde-derived V is shown in Fig. 7, in which the data pairs contaminated with rain are not included. The rms difference between the retrieved and radiosonde-derived V is 0.33 cm, 6% relative to the mean. No attempt was made, using radiosonde measurements as ground truth, to compare the accuracy of V retrieved using the methods with and without the corrections in $\bar{k}_{L,\nu}$ and $T_{mr,\nu}$. As indicated earlier, the improvement in V is minor and such a comparison is essentially pointless because the radiosonde-derived V contains errors comparable to those in retrievals. Unfortunately, due to the lack of ground truth, no similar comparison for the measurement of L is available.

It should be pointed out that even if the radiometer and ceilometer are collocated and pointed in the same direction, data from the two systems may not be matched, that is, cloud-free radiometric data with cloudy ceilometer data and vice versa. This problem is a result of the slightly different beamwidths and sensitivities of the two systems. The situation could be even worse if the antenna beams of the two system were misaligned. The discrepancy to the presence of clouds, however, is somewhat ameliorated by the 5-min data averaging. In this experiment about 14% of the radiometric data were mismatched with the ceil-

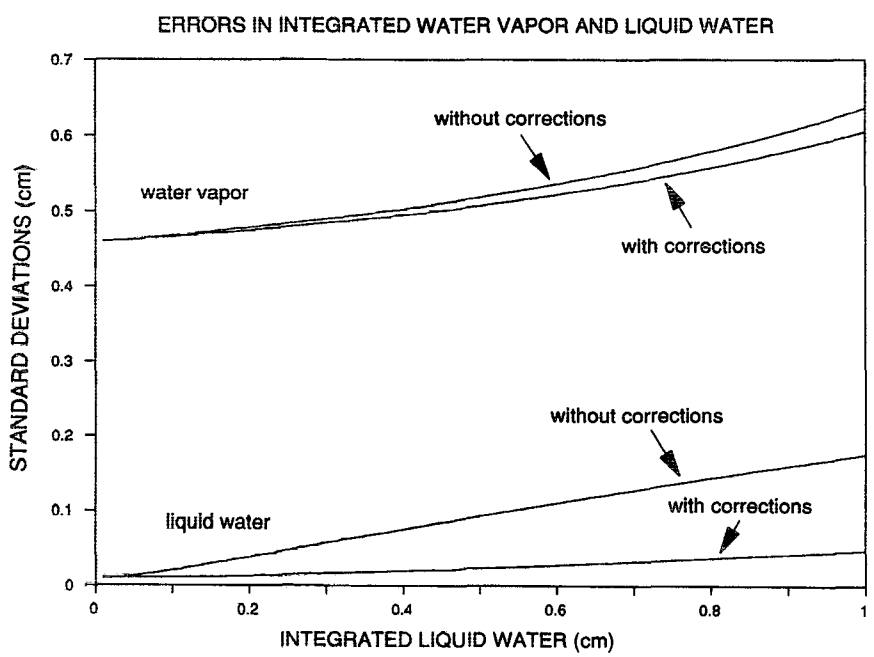

FIG. 5. Errors in integrated water vapor and liquid water retrieved by physical inversion techniques with and without corrections to $\bar{k}_{L,\nu}$ as function of integrated liquid water for a specified integrated water vapor 5.6 cm and cloud-base height 700 m.

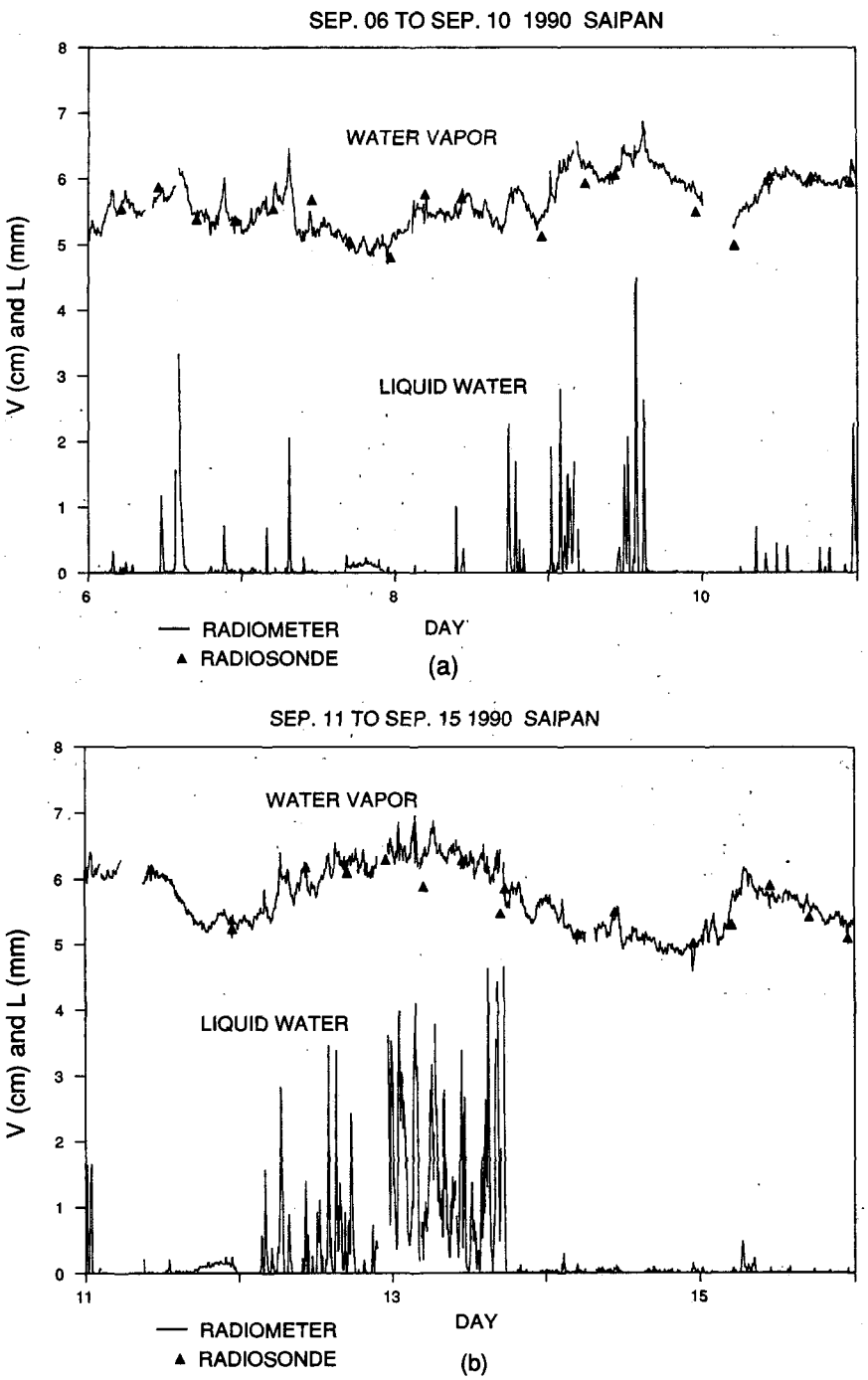

FIG. 6. Time series of radiometer-derived integrated water vapor, compared with that derived from radiosonde, and radiometer-derived integrated liquid water.

ometer data. For the inversion of these data, no corrections to $\bar{k}_{L,\nu}$ and $T_{mr,\nu}$ were made.

4. Limitations of temperature profile retrievals

The temperature profile information is contained in the set of the radiative transfer equations

$$T_{b,\nu} = T_{\mathrm{bb}} e^{-\tau_{\nu,\infty}} + \int_0^{\tau_{\nu,\infty}} T e^{-\tau_\nu} d\tau_\nu, \qquad \nu = \nu_1, \nu_2, \ldots, \nu_m. \tag{16}$$

It is well known that to obtain the temperature profile from these equations is an ill-posed mathematical

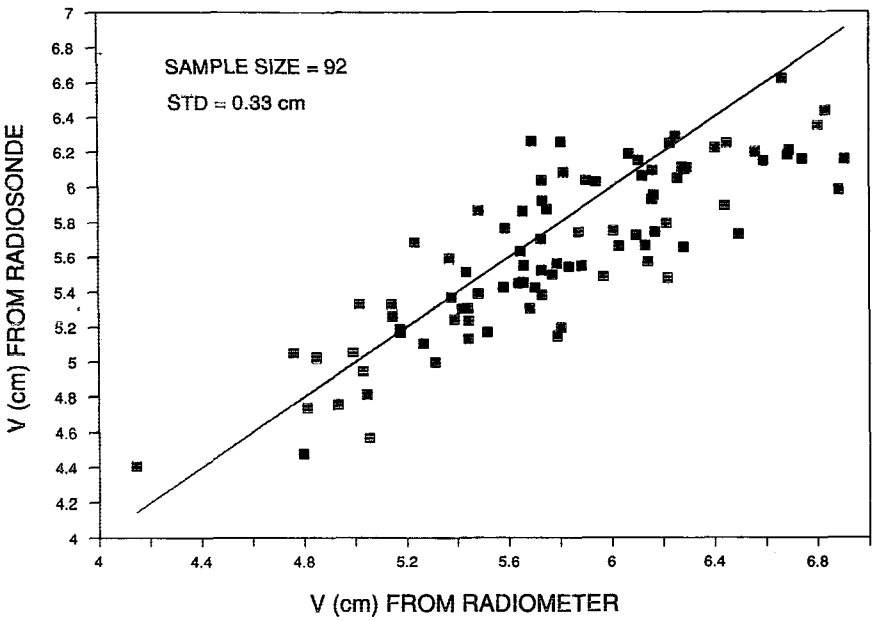

FIG. 7. Scatter diagram of radiometer- versus radiosonde-derived integrated water vapor.

problem as it can be seen that adding any profiles orthogonal to those weighting functions yields the same set of measurements. Therefore, additional knowledge about the temperature profiles is required to constrain the solution. The most commonly used constraint is statistical information, such as the climatological means and standard deviations, obtained from an a priori ensemble of temperature profiles and coincident radiometric measurements. Using such statistical inversion methods, an rms retrieval accuracy of about 1°–2°C can be achieved, but the vertical resolution is generally poor. At middle latitudes, climatological variations of the temperature profiles are relatively large; therefore, the radiometer provides significant information in determination of temperature profiles. However, the situation in the tropics is quite different. As shown in Fig. 2a, the standard deviation of the local temperature profiles during the experiment was only about 1°C. The situation is further illustrated in Fig. 8, which shows the standard deviation of the radiosonde temperature profiles and predicted rms retrieval errors, obtained from the same radiosonde profile ensemble at Guam mentioned in section 4. From the surface to 400 mb, the difference between the retrieval accuracies and the climatological variations is only 0.2°C. Note that in the calculation of the predicted errors, we have assumed that the statistical characteristics of the unknown temperature profiles were the same as those of the a priori temperature profile ensemble and the radiative transfer model for solving the forward problems was perfect. The experimental results, as discussed below, showed that the retrievals were essentially no better than a climatological mean.

The equation to derive the temperature profiles is the one similar to (7) but more general to include the surface temperature, pressure, and humidity. It may be written as (Rodgers 1976)

$$\hat{\mathbf{x}}' = E[\mathbf{x}'\mathbf{y}'^{\mathrm{T}}]E[\mathbf{y}'\mathbf{y}'^{\mathrm{T}}]^{-1}\mathbf{y}', \qquad (17)$$

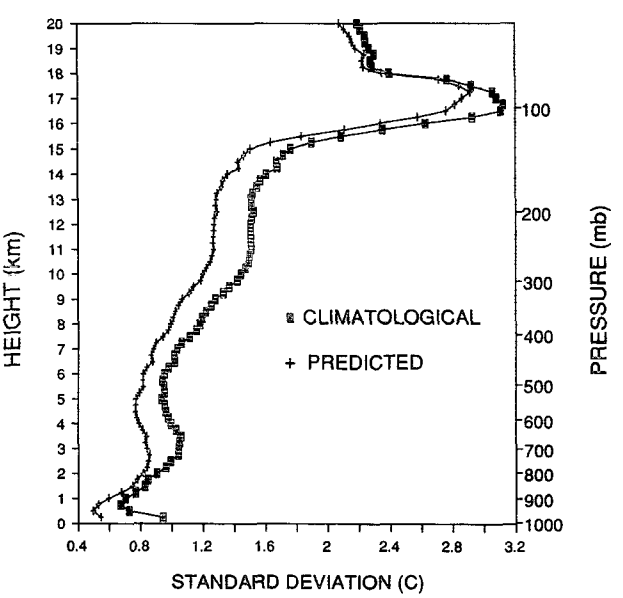

FIG. 8. Climatological variations and predicted retrieval errors of temperature profiles. Both were obtained from an a priori ensemble of radiosonde profiles at Guam in August and September from 1984 to 1988.

where x is the unknown temperature profiles, y is the measurement vector, and the quantities with a prime represent the departures from the means. The measurement vector y consisted of 11 components: brightness temperature measurements at five oxygen, two water vapor, and one liquid water sensitive channel, and measurements of the surface temperature, pressure, and relative humidity. The profile vector was made up of 86 components: 80 for the temperature profile from the surface to 20 km, four for geopotential heights at 850, 700, 500, and 400 mb, and two for integrated water vapor and cloud liquid. (The retrievals of the integrated water vapor and liquid using this retrieval technique will not be discussed below.) The statistical quantities in (17) were obtained from the a priori ensemble of radiosonde profiles at Guam. The radiometric measurements required for calculating these quantities were simulated using the radiative transfer model from the radiosonde profile ensemble.

Using radiosonde profiles launched during this experiment as ground truth, we compared the radiometer-derived temperature profiles with the climatological mean obtained from the a priori radiosonde profile ensemble. To account for the ascending period of the radiosonde, we averaged the radiometric measurements over 25 min, which was about the time period the balloon took to reach 400 mb. The erroneous data in the oxygen channels were removed when anomalous data were found in these channels or in the three vapor–liquid channels. Three rms error profiles were calculated, as shown in Fig. 9. All three curves are the differences between the estimated and the radiosonde-measured temperature profiles. The curve labeled "RETRIEVED" shows the errors in radiometer-derived temperature profiles. The curve labeled "THEORETICAL" represents the errors in the temperature profiles derived from the simulated radiometric measurements. The simulations were made by using the same radiative transfer model as that for constructing the inversion equation (17) and the radiosondes whose temperature profiles were used as the ground truth. The curve labeled "CLIM. MEAN" is the climatological mean at Guam. The overall rms differences below 400 mb were 1.28° (RETRIEVED), 1.14° (THEORETICAL), and 0.90°C (CLIM. MEAN). Thus, the accuracies of both radiometric and simulated retrievals were no better than that using a climatological mean.

Theoretically, if the statistical characteristics of the unknown temperature profiles and measurement vector are the same as those used to construct the inversion equation (17), the retrieved accuracy will always be better than that using the climatological mean, as shown in Fig. 8. However, in reality, the difference always exists, even when a representative radiosonde profile ensemble is used. There are uncertainties in the simulated radiometric measurements, especially when dealing with clouds. In this experiment, the geographic

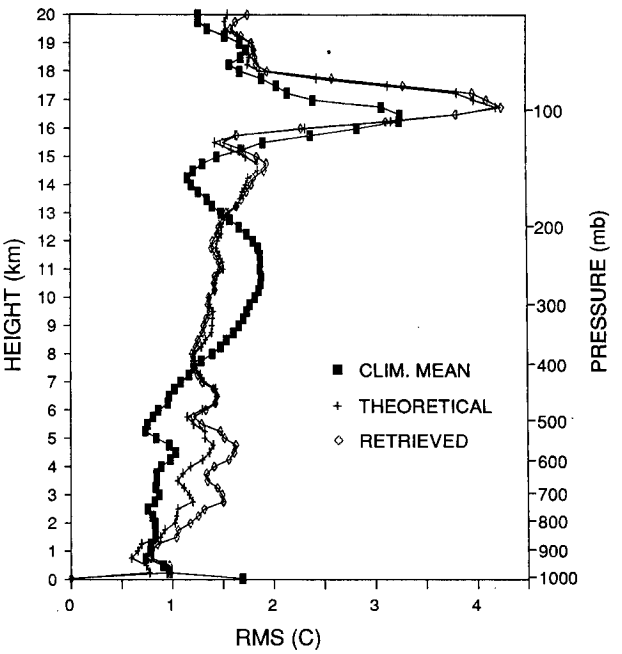

FIG. 9. Root-mean-square differences between estimated and radiosonde-measured temperature profiles during the TCM-90 experiment. "RETRIEVED" represents errors in radiometer-derived temperature profiles, "THEORETICAL" represents errors in the temperature profiles derived from the simulated radiometric measurements, and "CLIM. MEAN" represents errors in the temperature profiles estimated by the climatological mean at Guam.

separation between Saipan and Guam, adds another source to the disparity in the statistical properties at the two locations. Therefore, it can be understood that in a situation such as this, the retrievals may not be any more accurate than the climatological profiles since temperature variations are very small. It is also noted that since the geopotential heights were determined by the mean temperature between the surface and those heights and the surface pressure, any temporal variations in the retrievals were primarily associated with the variations in the surface pressure measurements.

The temperature retrieval accuracy obtained in this experiment seems to be comparable to or better than those achieved at middle latitudes. However, the radiometric measurements did not add more temperature information than was available in the climatological mean. Since the inversion method requires the statistical information, the radiometric measurements will be of no significance if the climatological variations are comparable to the retrieval errors.

5. Conclusions

We have presented results of the radiometric observations during the TCM-90 experiment in a tropical region. Statistical inversion techniques were applied to

both temperature profiles and integrated water vapor and cloud liquid. For the retrievals of integrated water vapor and cloud liquid, methods were developed to deal with the cloud-caused variations in cloud absorption coefficients and mean radiating temperatures. Error analyses have shown that these methods improve retrieval accuracies of L and, slightly, V. More than a 50% improvement in retrieval accuracy of the integrated cloud liquid can be gained with the corrections of cloud absorption coefficients. However, there was no ground truth available to verify the results.

Compared with radiosonde data, the integrated water vapor was accurate to 6% relative to the mean of 5.7 cm, and the temperature profiles below 400 mb were accurate to 1.28°C. However, the radiometer provided no new information for the temperature profile retrievals due to the fact that the climatological mean temperature profile, which was required by the statistical inversion technique, had represented the temperature profiles observed during this experiment.

Acknowledgments. The authors thank Dr. E. R. Westwater for valuable suggestions during the course of this work. We also thank J. B. Snider for his help in calibrations of the nine-channel radiometer. Professor John Reagan at the University of Arizona guided assembly of the radiometer package and design of the processing subsystem. His assistance is very gratefully acknowledged. This work was supported by the Office of Naval Research Grant N00014-86-K-0688.

REFERENCES

Albrecht, B. A., C. W. Fairall, D. W. Thomson, and A. B. White, 1990: Surface-based remote sensing of the observed and the adiabatic liquid water content of stratocumulus. *Geophys. Res. Lett.*, **17**, 89–92.

Hogg, D. C., F. O. Guiraud, J. B. Snider, M. T. Decker, and E. R. Westwater, 1983: A steerable dual-channel microwave radiometer for measurement of water vapor and liquid in the troposphere. *J. Climate Appl. Meteor.*, **22**, 789–807.

Liebe, H. J., 1985: An updated model for millimeter wave propagation in moist air. *Radio Sci.*, **20**, 1069–1089.

Politovich, M. K., B. B. Stankov, and B. E. Martner, 1992: Use of combined remote sensors for determination of aircraft icing altitudes. *Proc. 11th Int. Conf. on Clouds and Precipitation,* Montreal, Amer. Meteor. Soc., 978–982.

Rodgers, C. D., 1976: Retrieval of atmospheric temperature and composition from remote measurements of thermal radiation. *Rev. Geophys. Space Phys.*, **14**, 609–624.

Snider, J. B., F. O. Guiraud, and D. C. Hogg, 1980: Comparison of cloud liquid content measured by two independent ground-based systems. *J. Appl. Meteor.*, **19**, 577–579.

Thomson, D. W., 1988: New perspectives on atmospheric structure and dynamics. *Earth and Mineral Sciences,* 57 pp.

Westwater, E. R., 1978: The accuracy of water vapor and cloud liquid determination by dual-frequency ground-based microwave radiometry. *Radio Sci.*, **13**, 667–685.

——, M. T. Decker, and A. Zachs, 1983: Ground-based remote sensing of temperature profiles by a combination of microwave radiometry and radar. *J. Climate Appl. Meteor.*, **22**, 126–133.

——, W. B. Sweezy, L. M. McMillin, and C. Dean, 1984: Determination of atmospheric temperature profiles from a statistical combination of ground-based profiler and operational *NOAA 6/7* satellite retrievals. *J. Climate Appl. Meteor.*, **23**, 689–703.

——, J. B. Snider, and M. J. Falls, 1990: Ground-based radiometer observations of atmospheric emission and attenuation at 20.6, 31.65, and 90.0 GHz: A comparison of measurements and theory. *IEEE Trans. Antennas Propag.*, **38**, 1569–1580.